JOURNAL OF GEOPHYSICAL RESEARCH, VOL. 101, NO. A12, PAGES 27,431–27,442, DECEMBER 1, 1996

Testing the accuracy of magnetospheric model field line mapping

T. I. Pulkkinen

Finnish Meteorological Institute, Helsinki

N. A. Tsyganenko

Hughes STX Corporation, NASA Goddard Space Flight Center, Greenbelt, Maryland

Abstract. We present a new method to test the statistical accuracy of field-aligned mappings by using a large magnetospheric data set and apply the method to the *Tsyganenko* [1989] model. The obtained errors in the field-aligned mappings are generally small in the auroral zone outside the midnight sector but become larger on the nightside and within the polar cap. The model tail field is overstretched near midnight and the model field lines flare out toward the flanks and toward high Z values too much. The results also imply that there is a shear layer between the plasma sheet and lobe that could be indicative of the region 1 field-aligned current system. The large-scale mapping properties suggest that the magnetotail field is asymmetric with respect to the noon-midnight meridian: the model better represents the evening-sector field configuration, whereas the morning-sector model field lines map too far down the tail.

1. Introduction

The ongoing International Solar-Terrestrial Physics program hosts an unprecedented suite of satellites dedicated to magnetospheric studies [e.g., *Acuña et al.*, 1995]. While providing excellent opportunities for studying magnetospheric phenomena that are difficult to capture with single-satellite measurements, the program also sets strong demands for the analysis tools in order to reveal coherent events in the flow of highly variable multi-point data. As the particle motion is guided by the ambient magnetic and electric fields, the magnetic field models are particularly useful when observations from different regions of space are compared with each other.

Furthermore, the joint observation campaigns combining multi-satellite and ground-based measurements call for careful planning of the experiments in advance. Magnetic field models can be utilized to predict advantageous constellations of spacecraft and their conjunctions with ground stations. Such predictions have been effectively used in the planning of the coordinated ground-based measurement campaigns in conjunction with the ISTP satellite programs [e.g., *Lockwood and Opgenoorth*, 1995].

In order to achieve the above goals, the magnetic field models should provide sufficiently accurate mappings of the field lines also for instantaneous configurations during individual events. For this purpose, the average model parameters can be further adjusted to provide a best fit to local magnetic field measurements [e.g., *Pulkkinen et al.*, 1992] or to low-altitude precipitation data [*Sergeev et al.*, 1993], which can significantly improve the mapping accuracy in event studies.

The need to get both accurate field values and accurate field-aligned mappings from the models has given rise to studies where the accuracy of the models is tested using magnetic field measurements. *Fairfield* [1991] evaluated the *Tsyganenko* [1987] (T87) model and the model by *Tsyganenko and Usmanov* [1982] (TU82) using about 22000 magnetic field measurements. He concluded that the models tended to predict too large field values near the high-latitude cusps and near the tail equatorial plane and that the T87 model was in many respects superior to the earlier version. This study also suggested that the model tail field was not sufficiently stretched. On the other hand, *Peredo et al.* [1993] discussed the field values at the tail current sheet, and concluded that both the T87 and *Tsyganenko* [1989] (T89) models underestimated the current sheet B_Z, but that the value given by T87 corresponded better to the observed values. This study concluded that the models are on average too stretched in the nightside tail.

An experimental test of field-aligned mapping was performed by *Reeves et al.* [1996], who constructed data-based mappings between the ionosphere and geosynchronous orbit using measurements of particle spectra. Over 100 observational mappings were used to evaluate the predictive capability of the existing empirical field models (TU82, T87, T89, *Hilmer and Voigt* [1995],

Paper number 96JA02489.
0148-0227/96/96JA-02489$09.00

and *Olson and Pfitzer* [1977]). The result was that, on average, all the field models tended to be too stretched but that the variance was quite large, and that none of the models performed markedly better than the others. This study mainly concentrated on relatively quiet periods when good spectral matches could be obtained.

In this paper, we study possible systematic errors in the T89 model mapping from the high-latitude ionosphere to distant regions of the magnetosphere. We introduce a perturbation technique, in which the observed magnetic field vectors are used for evaluating the difference between the actual field direction and that given by the model. Section 2 describes the method, and in section 3 we show results of calculating the mapping errors. In the Discussion section we summarize our findings and their physical implications. The described method is quite general and can be applied to any magnetic field model.

2. Calculation of the Errors in Field-Aligned Mappings

In order to evaluate errors in field-aligned mappings, the field direction must be observed along the entire field line. To that end, the magnetic field measurements from the large magnetospheric database [*Fairfield et al.*, 1994] were binned into subsets each representing a flux tube which crosses the ionosphere at a given latitude and local time range. Along each flux tube, vector differences between the observed and model field directions were computed. The integrated effect of the vector differences along the entire flux tube was used as a measure of the mapping error, and the resulting correction vector as an indicator how to correct the model prediction of the mapping.

2.1. Derivation of Correction Vectors

For data binning purposes, we divided the Earth's surface into $(\Delta\phi, \Delta\lambda)$ bins, where ϕ and λ are the solar magnetic (SM) latitude and longitude, respectively. In the SM coordinate system the Z axis is directed northward along the dipole axis, the X axis lies in the plane defined by the dipole axis and the Sun-Earth line, and the Y axis points duskward, completing the right-handed triad. The footpoint binning results in a finite number of flux tubes, so that each data point in the database is associated with only one flux tube.

Let us denote $\mathbf{b}_a(\mathbf{r})$ the unknown actual (hence the subscript a) direction of the magnetic field at a point $\mathbf{r}$. Tracing the actual field line from the middle of a $\Delta\phi - \Delta\lambda$ bin (located at $\mathbf{R}_0$) to some distance S from the Earth leads to the point

$$\mathbf{R}_a(S) = \mathbf{R}_0 + \int_0^S \mathbf{b}_a(\mathbf{r}_a(s))\, ds, \qquad (1)$$

where s is the distance from the ionosphere (100 km altitude) along the field line. Similarly, tracing the field line from the same footpoint but using the model field direction $\mathbf{b}_m = \mathbf{B}_m/B_m$ leads to the point

$$\mathbf{R}_m(S) = \mathbf{R}_0 + \int_0^S \mathbf{b}_m(\mathbf{r}_m(s))\, ds. \qquad (2)$$

The error in the field-aligned mapping is then the vector difference between the end points $\Delta\mathbf{R}(S) = \mathbf{R}_a(S) - \mathbf{R}_m(S)$. The top sketch of Figure 1 illustrates the tracing geometry.

Assuming that the difference between the actual and model field lines is small, we can use the model integration path $\mathbf{r} = \mathbf{r}_m(s)$ in equation (1) instead of the actual integration path $\mathbf{r} = \mathbf{r}_a(s)$. With this assumption, the total error $\Delta\mathbf{R}(S)$ is given by

$$\begin{aligned} \Delta\mathbf{R}(S) &= \int_0^S (\mathbf{b}_a(\mathbf{r}_m(s)) - \mathbf{b}_m(\mathbf{r}_m(s)))\, ds \qquad (3) \\ &= \int_0^S \delta\mathbf{b}(s)\, ds, \end{aligned}$$

where $\delta\mathbf{b}(s) = \mathbf{b}_a(\mathbf{r}_m(s)) - \mathbf{b}_m(\mathbf{r}_m(s))$, and the integration is made along the model field line, which is known.

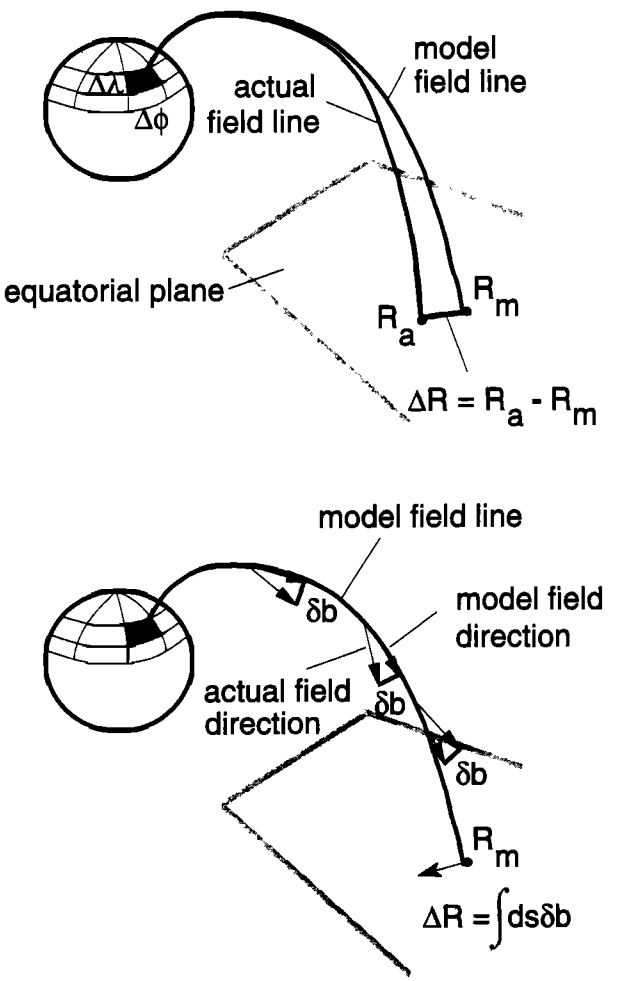

Figure 1. A schematic illustration of the error estimation method. For details see the text.

The total error $\Delta\mathbf{R}$ can now be integrated if we can define the deviation vectors $\delta\mathbf{b}(s)$. Although the actual field direction along the model field line $\mathbf{b}_a(\mathbf{r}_m(s))$ is still unknown, both $\mathbf{b}_a$ and $\mathbf{b}_m$ are known at the locations $\mathbf{r}_i(s)$ of the data points inside the flux tube. We can therefore evaluate the deviation vectors

$$\delta\mathbf{b}(\mathbf{r}_i) = \mathbf{b}_a(\mathbf{r}_i) - \mathbf{b}_m(\mathbf{r}_i) \quad (4)$$

for all data points $\mathbf{r}_i$ $(i = 1, ..., N)$. Using these data points, the s dependence of $\delta\mathbf{b}$ can be approximated by an analytical function of s with free parameters, whose values can be evaluated by least squares, provided that the number N of data points in the flux tube is sufficiently large. The derived analytical approximation for $\delta\mathbf{b}(s)$ can then be substituted in equation (3) to find the cumulative mapping error $\Delta\mathbf{R}(S)$. The bottom sketch in Figure 1 illustrates derivation of the error from the deviation vectors.

2.2. Binning of the Database

The data used in this study are the approximately 79,000 vector magnetic field measurements from 11 space missions compiled by *Fairfield et al.* [1994]. The data are mostly 0.5 R_E averages along the spacecraft trajectory, which near the satellite apogee can mean up to 30-min averages (see *Fairfield et al.* [1994] for details of the averaging procedures). Each of the data points has been tagged with hourly averages of solar wind and interplanetary magnetic field data when available.

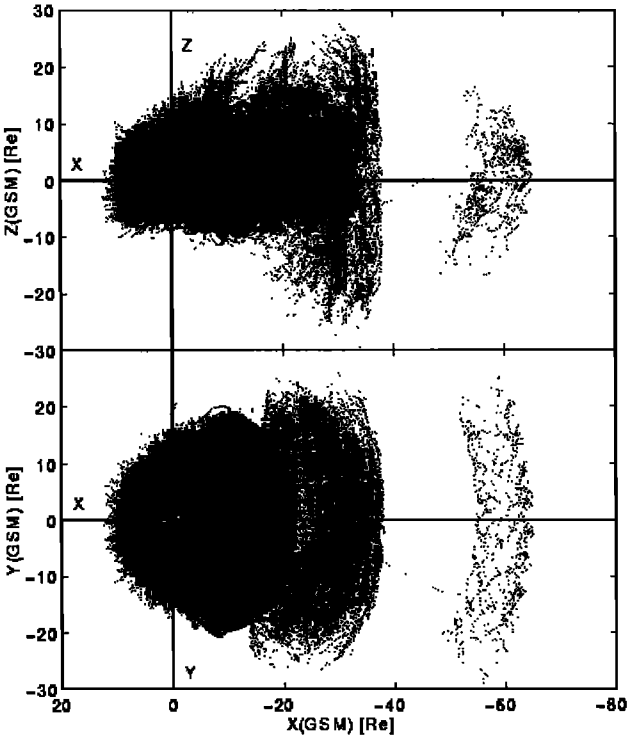

Figure 2. Distribution of data points in the *Fairfield et al.* [1994] data set. Two projections are shown: (top) The noon-midnight meridian plane and (bottom) the equatorial plane.

First, the data set was divided into six subsets corresponding to the same Kp intervals ($Kp = 0, 0+$, $Kp = 1-, 1, 1+$, $Kp = 2-, 2, 2+$, $Kp = 3-, 3, 3+$, $Kp = 4-, 4, 4+$, $Kp > 5-$), as those used in calibrating the T89 model. Figure 2 shows the distribution of data points in the entire data set, projected onto the geocentric solar magnetospheric (GSM) $X - Z$ and $X - Y$ planes. A correction for the standard 4-deg aberration has been applied to the data point positions and the magnetic field components.

We assumed that the magnetospheric field components have the following inversion symmetry with respect to the dipole tilt and the GSM Z-coordinate [e.g.,*Mead and Fairfield*, 1975]

$$\begin{aligned} B_X(X,Y,-Z,\Psi) &= -B_X(X,Y,Z,-\Psi) \\ B_Y(X,Y,-Z,\Psi) &= -B_Y(X,Y,Z,-\Psi) \\ B_Z(X,Y,-Z,\Psi) &= B_Z(X,Y,Z,-\Psi). \end{aligned} \quad (5)$$

These symmetry relationsips hold for the field of the Earth's dipole in the aberrated GSM coordinates, and there is no physical reason for a violation of the symmetry in the actual average magnetospheric configuration. For example, the central surface of the tail current sheet, warped in two dimensions for any negative value of the dipole tilt angle, should be a mirror reflection in the plane $Z_{GSM} = 0$ of the same surface for a positive tilt angle. Under this assumption, there is no need to separately estimate the mapping errors in the northern and southern hemispheres. Rather, it suffices to "convert" all southern hemisphere data points into northern ones by using the symmetry relations in equation (5), and then to perform the integration in equation (3) only along the northern hemisphere flux tubes. Here the "southern hemisphere data points" are those lying southward of the warped surface $Z = Z_s(X, Y, \Psi)$, defining the T89 model equatorial current sheet.

Within each Kp subset, all data points were mapped to the ionosphere (at 100 km altitude) using the corresponding T89 model, and the footpoints were transformed to SM coordinates. Each magnetic field measurement was then associated with a field line length s, SM latitude, and SM longitude of the footpoint.

As a result of imperfections of the model, a small number of distant data points mapped to outside the magnetosphere in both directions and hence did not have ionospheric footpoints. Such data points were left out of this study. Figure 3 shows the distribution of ionospheric footpoints in solar-magnetic coordinates for the subset with $Kp = 3$. Because the data set did not contain measurements inside $\sim 4R_E$, there are no footpoints equatorward of $\sim 60°$ SM latitude.

In addition to the geomagnetic activity conditions, the magnetospheric field configuration depends also on the Earth's dipole tilt angle Ψ. However, binning the

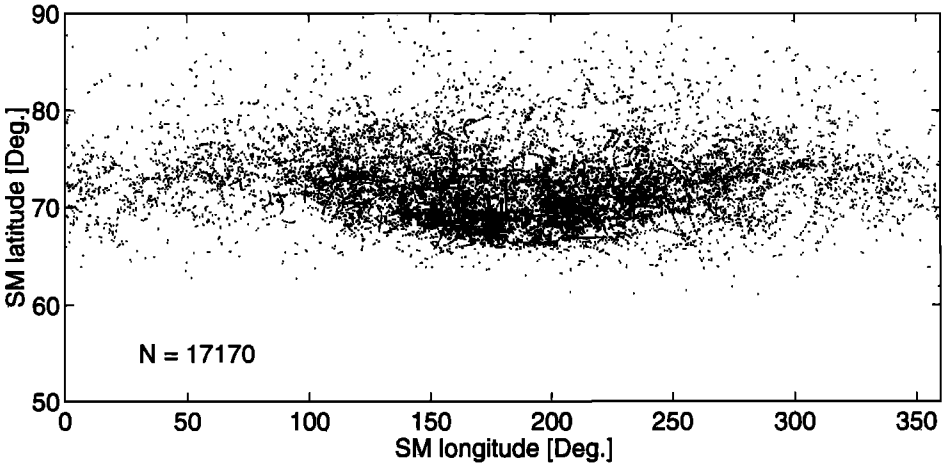

Figure 3. The ionospheric footpoints of the data points in the data set for $Kp = 3$. Note that there are no data points equatorward of about 60°.

data set into several Ψ intervals would lead to too small a number of data points in each latitude – longitude bin. For that reason, we combined data points with different values of Ψ, as long as the field line footpoints fell within the same interval of SM latitude and longitude in the ionosphere. This convention implies a relatively weak dependence of the systematic deviation vector $\delta\mathbf{b}$ defined by equation (4) on the dipole tilt angle. This assumption is based on the fact that the principal magnetospheric structures (ring current, plasma sheet, polar cusps, and the field-aligned currents) map to approximately same SM latitudes in the ionosphere for different values of the tilt angle Ψ. This result is supported both by observations [e.g., *Newell and Meng*, 1988] and by model calculations [e.g., *Tsyganenko*, 1990]. Furthermore, because the data are evenly distributed over all tilt angle values, combining all tilt angles does not cause any systematic errors in our analysis.

The size of the latitude-longitude bins was determined based on a tradeoff between having enough data points within any given flux tube and having enough spatial resolution to separate morphologically different flux tubes from each other. In this study, two binning grids were employed. Large-scale general features were examined using a rather coarse binning, in which the entire high-latitude region including the auroral zone and the polar cap was divided into three latitude intervals (60°–72°, 72°–78°, 78°–90°) and four MLT-sectors (0000–0600, 0600–1200, 1200–1800, 1800–2400). The latitudes were chosen to roughly separate open field lines (most poleward bins) and closed field lines (most equatorward bins), the latitude band 72°–78° contains both open and closed field lines. In addition, the lower-latitude regions were examined by using a finer gridding (five latitude bins 63°–66°, 66°–69°, 69°–72°, 72°–75°, 75°–78° and 12 two-hour-wide MLT bins). Above the latitude of ~78°, there were not enough datapoints to allow a finer binning. Figure 4 shows the number of datapoints within each bin for the $Kp = 3$ data set, for both the coarse and fine binning options.

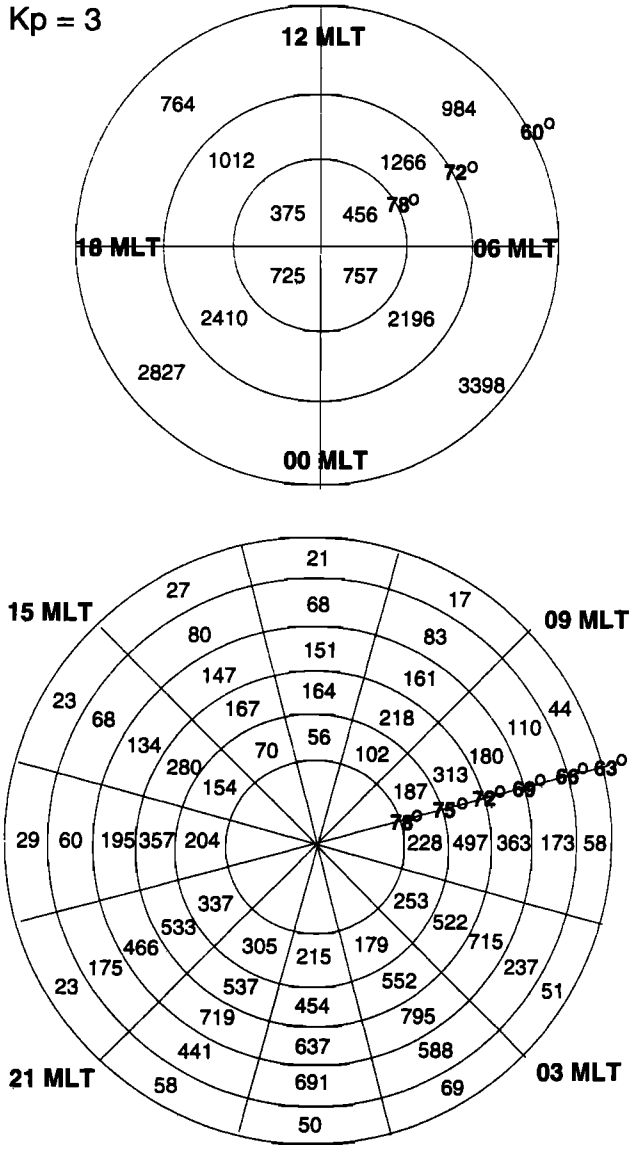

Figure 4. Two different binnings in latitude and longitude used to evaluate the mapping errors. The numbers give the number of data points within the flux tubes (distributed along the field line length) in the $Kp = 3$ data set.

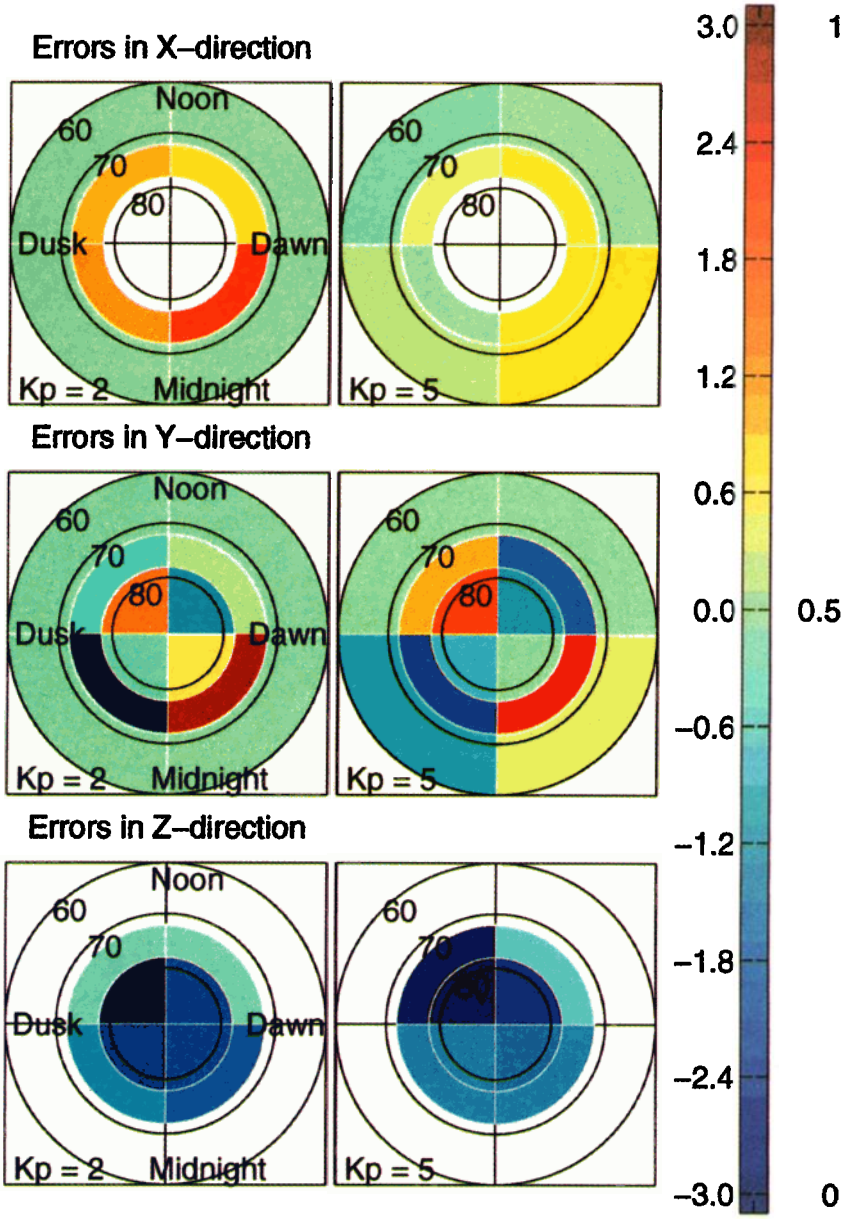

Plate 1. Statistical deviations in the field-aligned mappings using the coarse grid. The color coding in each bin corresponds to the deviation in mapping from the ionosphere to a reference plane in the magnetotail ($X = -50R_E$ for open field lines, equatorial plane for closed field lines). The deviations are given in units of R_E.

2.3. Analytical Approximations for the Correction Vectors

After the data set was divided into Kp subsets and binned into the latitude-longitude intervals according to their ionospheric footpoints, each point within a given flux tube was characterized by three components of the deviation vector $\delta\mathbf{b}$ and the coordinate s, corresponding to the distance of the measurement point from the ionosphere along the field line.

Figure 5 shows the Y and Z components of the deviation vectors $\delta\mathbf{b}$ as a function of s for the $Kp = 3$ subset, with the footpoint latitude-longitude bin centered at (84°,135°). The outer limit of integration has been set to $S = 50R_E$, since the number of datapoints beyond that distance is very small (see Figure 2).

For each flux tube, the components of the deviation vector were approximated by analytical functions, whose parameters were least squares fitted to the sets of measured deviations $\delta\mathbf{b}_i$. At low altitudes, the deviations rapidly fall off to zero for $s \rightarrow 0$, because the contribution from the Earth's dipole becomes much larger than the field from external sources. This imposes a restriction on the choice of the analytical forms for $\delta\mathbf{b}$. After trying several alternatives, we chose the following fitting functions:

$$\delta b_i = \tan^{-1}\left(\frac{s}{s_d}\right) \sum_{n=0}^{k} a_n s^n \qquad (6)$$

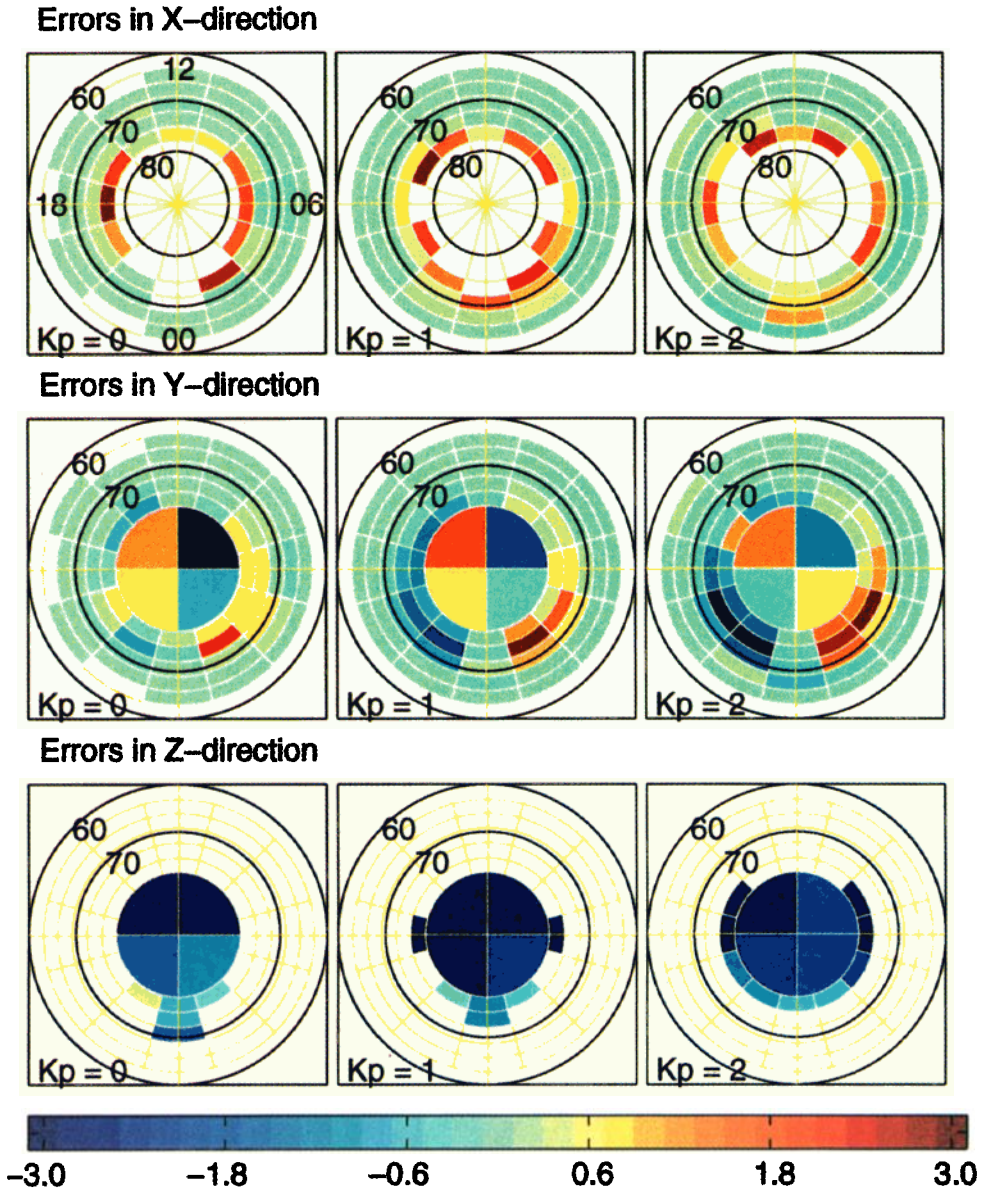

Plate 2. Statistical deviationss in the field-aligned mappings for $Kp = 0, 1, 2$ using the fine grid. The color coding in each bin corresponds to the deviation in mapping from the ionosphere to a reference plane in the magnetotail ($X = -50R_E$ for open field lines, equatorial plane for closed field lines). The deviations are given in units of R_E.

where $s_d = 5R_E$, $k = 3$, $i = X, Y, Z$, and different coefficients a_n were derived for each of the vector components.

As is evident from Figure 5, the correction vector values have a broad distribution of values, approximately centered around zero. Zero average of the distribution would indicate that the model gives a perfect description of the average field configuration, and that only random field variability causes errors in the mapping between high and low altitudes. However, especially in the lower panel it is evident that the best fit curve is not a zero line, and thus there is a systematic deviation of the model from the average field configuration. The best representation of the average error was found using equation (6) and a least squares fitting to determine the coefficients a_n. The solid curves in Figure 5 show the analytic representations of $\delta \mathbf{b}_Y$ and $\delta \mathbf{b}_Z$ given by equation (6) that give the best fit to the data in the least squares sense.

After the evaluation of the coefficients a_n, the analytical functions $\delta \mathbf{b}$ were analytically integrated to give the total deviation vectors $\Delta \mathbf{R}$. These vectors were then projected either on the equatorial plane for closed field lines, or on the $Y - Z$ plane for open field lines. Field lines were considered open if they crossed the equatorial plane outside of $R = 80R_E$. Integration of the functions drawn in Figure 5 yielded $\Delta R_Y = -0.3R_E$ and $\Delta R_Z = -1.5R_E$. This indicates that the T89 model maps the field line about 1.5 R_E too high in the Z direction.

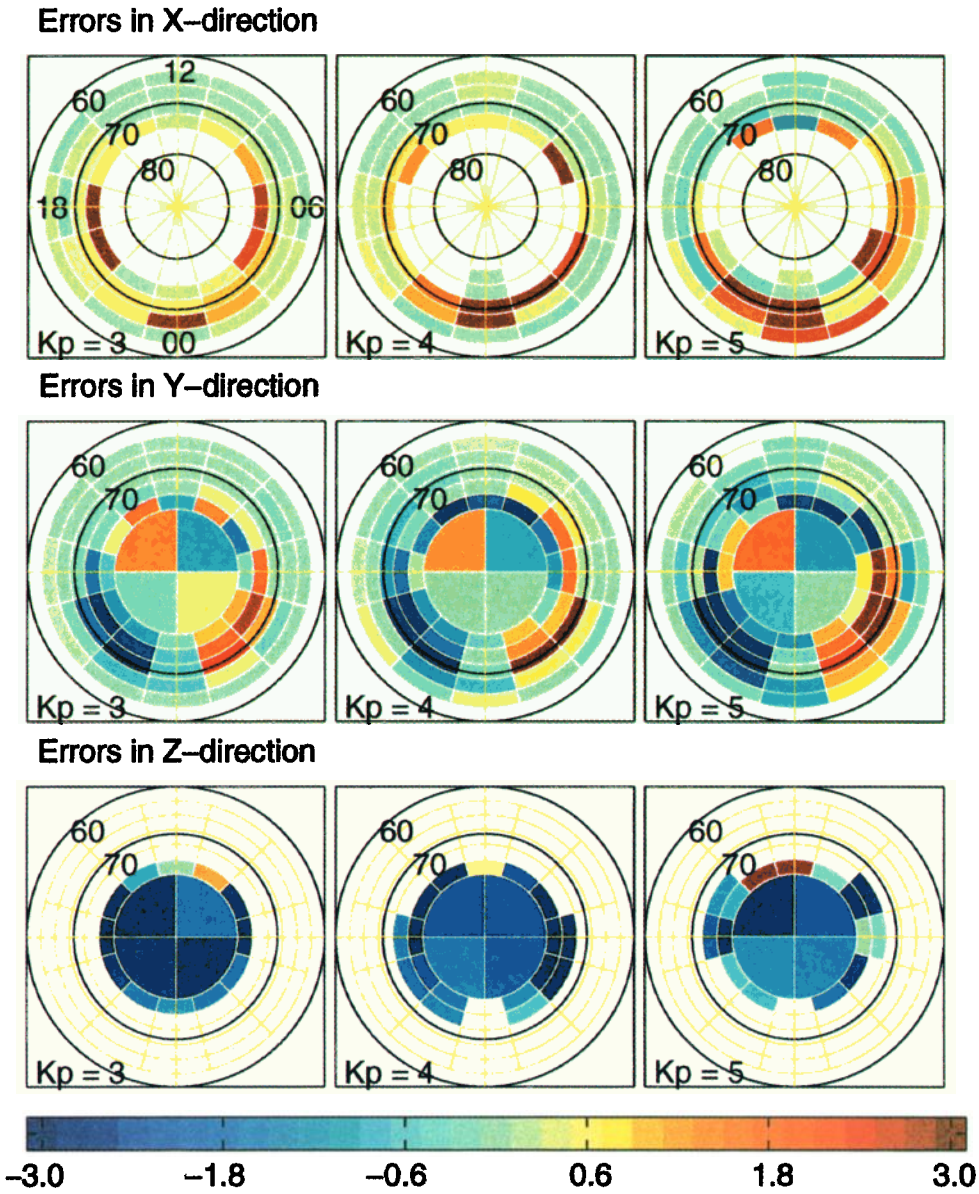

Plate 3. Statistical deviations in the field-aligned mappings for $Kp = 3, 4, 5$ using the fine grid. The color coding in each bin corresponds to the error in mapping from the ionosphere to a reference plane in the magnetotail ($X = -50 R_E$ for open field lines, equatorial plane for closed field lines). The deviations are given in units of R_E.

3. Analysis of Errors

3.1. Large-Scale Features

The coarse grid with three latitude bands and four local time sectors was used to examine the large-scale features in the error distributions. As all these bins include datapoints from a large spatial area in the magnetotail, the systematic trends in the results are more important than the actual numbers obtained. The latitudes were binned so that in the most equatorward bins all field lines are closed, whereas in the most poleward bins all field lines are open. The middle bins contain both open and closed field lines. Here open field lines were defined as those whose equatorial crossing point is outside 80 R_E in the tail.

3.1.1. Errors in the Y direction. The middle row in Plate 1 shows the errors in the Y direction for two Kp ranges, $Kp = 2$ and $Kp = 5$. Each bin is color-coded, according to the average mapping error in tracing that bin from the ionosphere to the magnetotail. The errors given in units of R_E represent the deviation of the average field line endpoint (as deduced by the method outlined in section 2) from the model one. The total deviation vectors given by equation (3) were projected either on the equatorial plane (for closed field lines) or on the tail cross-section plane (for open field lines). The Y component of the deviation vector does not depend on the projection plane and can be defined for all bins.

At low latitudes (SM latitudes 60°–72°), the Y-errors

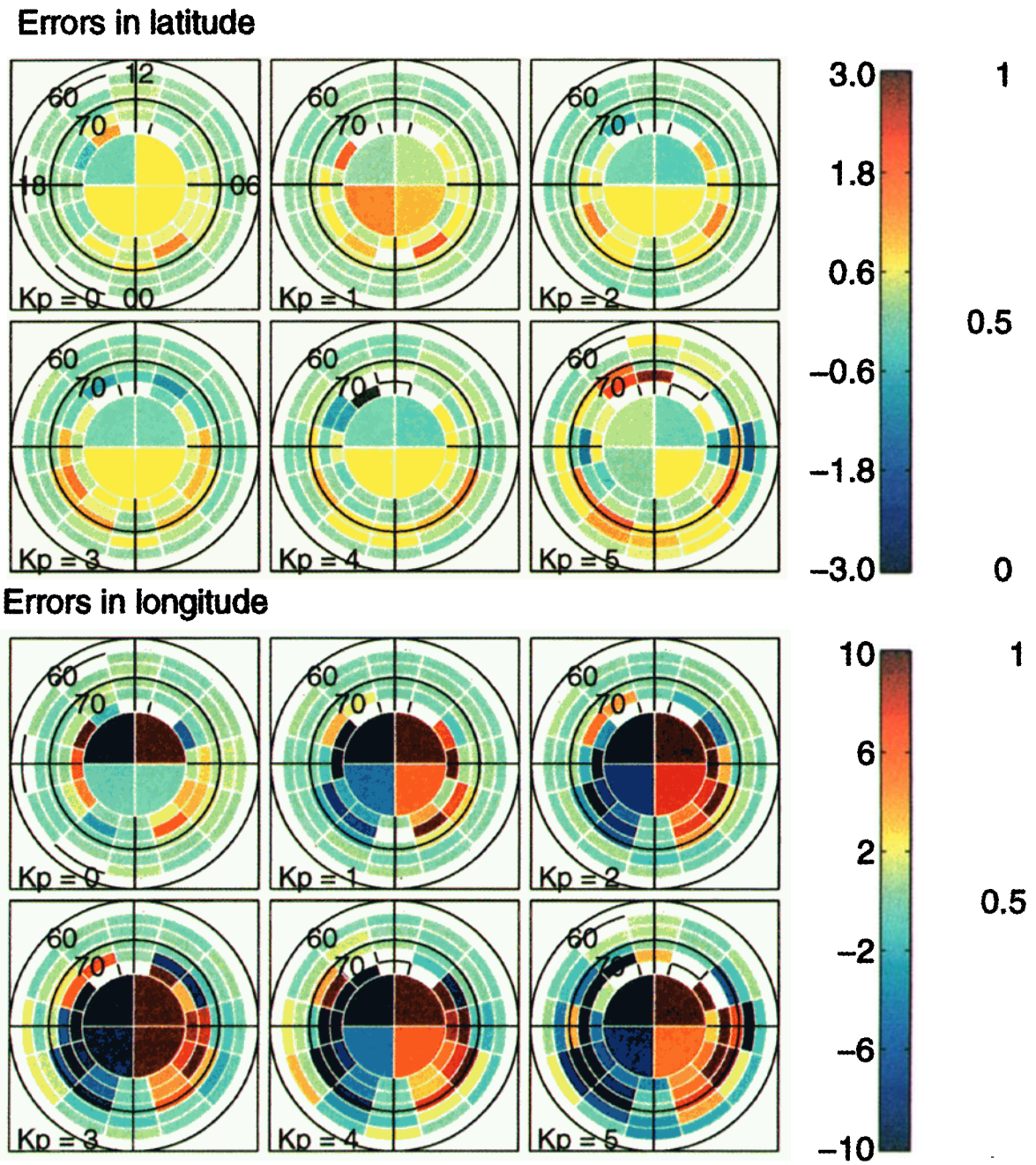

Plate 4. Statistical deviations in the field-aligned mappings for $Kp = 0, 1, 2, 3, 4, 5$ using the fine grid. The color coding in each bin corresponds to the error in mapping from the magnetotail to the ionosphere. The deviations are given in degrees. The white bins correspond to cases where the model maps the corrected location of the field line outside the magnetosphere. This can occur near the cusp location where the errors are large and the field lines are close to the magnetospheric boundaries.

are small for all Kp values (all Kp values not shown). The only exception is the case of largest activity, the $Kp = 5$ data set. In the nightside bins, the deviations are negative in the premidnight sector and positive in the postmidnight sector, indicating that the model field lines flare too much toward the flanks at these latitudes (i.e., the model field lines go to larger $|Y|$ values than implied by the data).

In the latitude region 72°–78°, the Y errors are generally much larger. On the nightside, the deviation tends to be negative in the premidnight sector and positive in the postmidnight sector, which again indicates that the model field lines flare too much in this latitude band. This is apparent even for the lowest activity ($Kp = 0$) data set, and the effect becomes larger for the higher activity levels.

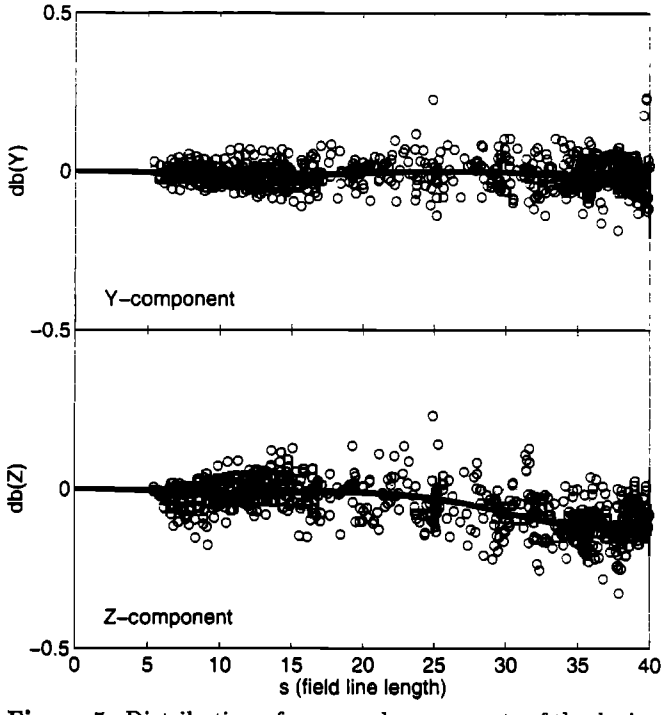

Figure 5. Distribution of measured components of the deviation vector δb_Y and δb_Z as a function of s (circles) ($Kp = 3$; lat = 78°–90o; MLT = 1800–2400). The solid line shows the analytical best fit functional representation of the deviation components.

Within the polar cap at latitudes >78°, the dayside Y-deviations are positive in the afternoon sector and negative in the prenoon sector. This indicates that the model underestimates the field flaring in the high-latitude polar cap. The nightside polar cap (lobe center) field lines do not show as coherent behavior. The errors are generally relatively small, and they are not consistently in one direction for all levels of activity.

3.1.2. Errors in the Z direction. The bottom row in Plate 1 shows the deviations in the Z direction in the high-latitude regions. The deviations in the Z direction were calculated only for field lines whose equatorial crossing points were outside $80R_E$. For this reason, the errors in the low-latitude bins were not plotted.

Within the polar cap (latitudes >78°) the Z deviations are consistently negative for every local time bin, indicating an excessive north-south flaring of the field lines for all activity levels. The largest errors are observed in the dayside afternoon sector, for the field lines that map close to the plasma mantle near the high-latitude boundary of the magnetotail. In the latitude band 72°–78°, the deviations are generally negative, with a few exceptions in the $Kp = 0$ and $Kp = 5$ data sets, where they are small and positive.

3.1.3. Errors in the X direction. The top row in Plate 1 shows the errors in the X direction in the two lowest latitude bins. For the higher-latitude open tail field lines the error in the X direction is not defined. At low latitudes, the errors are generally very small, with the exception of the postmidnight sector for the highest activity data set.

For the $Kp = 5$ data set, deviations in the postmidnight sector are positive, indicating that the model field is overstretched, that is, that the model field lines map too far tailward. As will be shown below in a more detailed plot, this is a general feature of the nightside tail. However, it is interesting to note that, on the large scale, this reveals a significant dawn-dusk asymmetry in the tail field, with a larger stretching of the field lines on the dusk side.

At higher latitudes, the deviations are larger and generally positive. Here it is also apparent that the postmidnight sector deviations are larger than the premidnight ones. Since the T89 model is symmetric with respect to the midnight meridian, this suggests that the field configuration in the evening sector is better represented by the model, while in the morning sector the model field lines are somewhat overstretched.

3.2. Mapping Errors in More Detail

Plates 2 and 3 show a summary of the detailed examination of the mapping errors in the same format as in Plate 1. Here the detailed grid is shown up to 78° latitude, poleward of that only one latitude bin and four local time sectors are shown in order to retain sufficient number of data points within each bin. Plate 2 shows the three lowest levels of magnetic activity ($Kp = 0, 1, 2$), whereas Plate 3 shows the three highest activity levels ($Kp = 3, 4, 5$). For the errors in the X direction, only bins that are on closed field lines (model field crosses the equatorial plane inside 80 R_E) are shown. Correspondingly, for the errors in the Z direction, only the open field line region is shown.

Although the general features discussed above are evident also in Plates 2 and 3, having more spatial resolution also increases the errors from those revealed in the very coarse data binning. It is easy to see in Plates 2 and 3 that the errors become much larger when the level of activity increases. Furthermore, whereas in the lowest-activity data sets the errors are relatively small at low latitudes (≤69°), the errors increase also in these bins for the higher activity cases. There is a clear day-night asymmetry: the dayside errors are much smaller than the nightside errors.

The most poleward bins near the noon sector exhibit somewhat larger errors than the other dayside regions. This could be indicative of the mapping difficulties near the polar cusps; large errors should be expected if a small deviation in field direction converts a dayside field line to a nightside tail field line. However, the location of the cusp is not well outlined in these error estimation plots.

3.2.1. Errors in the Y direction. The excessive flaring of the model field toward large $|Y|$ values is clearly revealed as negative deviations in the premidnight sector and positive deviations in the postmidnight

sector in Plates 2 and 3. With more latitudinal resolution, it is apparent that the errors maximize near the ionospheric latitudes corresponding to the plasma sheet boundary and become smaller both in the polar cap and at low latitudes. This could possibly indicate the influence of the Region 1 field-aligned current system not included in the T89 model.

3.2.2. Errors in the X direction. With a few exceptions, the errors in the X direction are positive in Plates 2 and 3. Better latitudinal coverage reveals a clear evolution of relatively small errors in the lowest latitude bins and increasingly larger errors in the higher latitude bins. It is also clear that the errors are larger in the nightside and especially near midnight. Thus the model field is too stretched. The asymmetry between the morning and evening hours is not as obvious in these results, but it does exist.

The X errors clearly become larger in the higher-activity data sets, and for these cases the errors are larger also in the lowest latitude bins that map close to geostationary orbit.

4. Discussion

In this paper we have developed a method that utilizes the large magnetospheric database described by *Fairfield et al.* [1994] to study the statistical accuracy of magnetic field models. By statistical accuracy or statistical error we mean differences that are apparent when the observed magnetic field directions within a pre-defined flux tube are compared with those predicted by the model. Any errors that are introduced due to magnetospheric activity or solar wind conditions not represented by the model current systems are averaged out in these results. Thus the total error in a given event consists of both the statistical error examined here and an activity dependent error [see, e.g., *Pulkkinen et al.*, 1992]. Moreover, the data set contains averages over 0.5 R_E of the spacecraft trajectory, or up to 30-min temporal averages. This data set is thus well-suited for evaluating statistical field models, when the largest short-lived peak values have already been averaged out from the data itself.

The method to estimate the statistical errors is independent of the magnetic field model. Thus, any field model can be tested by using the method developed here. The only limitation is the availability of a sufficient number of measurement points within each flux tube. Here we divided the data set into six subsets according to the Kp value, but combined all tilt angles into the same binning. This gave a sufficient number of data points in most 3° by 30° bins poleward of 63° SM latitude. Various binnings of data were examined in addition to the two presented in this paper. As long as the number of data points in each bin was sufficiently large, the results were independent of the binning. The data coverage in the magnetotail is sufficiently uniform so that sampling effects or uneven data distribution should not have affected our results.

As the T89 models are widely used in various applications of magnetospheric research, their statistical accuracy is of particular importance. Below we summarize our results of the error analyses and discuss their physical interpretation. Plates 2 and 3 can be used as a reference guide to estimate the expected mapping errors from different latitude/local time bins.

The mapping accuracy at low latitudes (equatorward of $\sim 69°$) and on the dayside is generally quite good, with a typical error less than $1R_E$. On the other hand, the results indicate that the model tail field flares out too much both in the Y and Z directions. Because magnetic flux is conserved in the tail, this also indirectly indicates that the model underestimates the lobe field at large radial distances. *Pulkkinen et al.* [1995] obtained similar results by comparing the distant tail field measurements with the T89 model. A model for the distant tail field developed by *Pulkkinen et al.* [1996] suggests that the tail field decreases from about 14 nT at $X = -50R_E$ to about 10 nT at $X = -100R_E$, and remains approximately constant to at least $\sim$200 R_E (see also *Slavin et al.* [1985] and *Yamamoto et al.* [1994]).

Furthermore, as has been discussed earlier [*Peredo et al.*, 1993; *Reeves et al.*, 1996], the model tail field lines extend too far down the tail equatorial plane, that is, the model field is overstretched. The overstretching is strongest near the midnight meridian (where the T89 model currents maximize) and is most significant for higher levels of activity. Apparently the errors are largest in the midtail region: in the equatorwardmost and polewardmost closed field line bins the errors are quite small even for the larger activity data sets.

The T89 model is symmetric with respect to the midnight meridian. The difference in the error values in the premidnight and postmidnight sectors indicates that there is an asymmetry in the field such that the field lines in the premidnight sector map further down the tail than in the postmidnight sector. Furthermore, it seems that the T89 models are more consistent with the premidnight sector observations, as the errors in the postmidnight sector are larger. This is especially apparent during strong magnetospheric activity during which the cross-tail current and ring current are substantially enhanced above their quiet time values. As the magnetic drifts in the near-Earth tail are dependent on particle charge and energy, the asymmetry probably arises from the different drift paths of electrons and protons around the Earth [e.g., *Erickson*, 1992]. The question of why the models weight the observations differently giving better results in the premidnight sector is beyond the scope of this paper.

An interesting point is that the nightside Y errors seem to be concentrated at latitudes corresponding to the expected position of the outer boundary of the plasma sheet. The errors maximize in the latitude bin

69°–72° for all activity levels and become small or even reverse poleward of 78°.

The sign of the deviations indicates a deflection of the tail field lines toward the midnight meridian plane, which can be attributed to electric currents flowing nearly parallel to the tail axis. When mapped to the ionosphere, the sense of these currents (earthward at $Y<0$ and tailward at $Y>0$) as well as the latitudinal position of the maximal error region are consistent with those of the region 1 Birkeland current system [e.g., *Iijima and Potemra*, 1976], whose contribution is not represented by the T89 model (see also *Tsyganenko et al.* [1993]). The region 2 currents probably do not show up as errors in the lower-latitude bins because in that region the background field is much stronger, which decreases the relative importance of the field-aligned currents.

Often the field-aligned mappings are made from the magnetosphere down to ionospheric altitudes, and it would be desireable to know what the errors involved are in latitude and longitude. In order to illustrate that we have mapped the error vectors from the tail to the ionosphere. The difference of the footpoint of the error vector and the bin center then gives an estimate of the error in latitude and in longitude. Plate 4 shows a map similar to Plates 2 and 3, but now the color coding shows the ionospheric errors in degrees of latitude and longitude. (Note that the latitude and longitude plots have different scales.) The features found in this plot are similar to those in Plates 2 and 3, although the convergence of the field results in slightly smaller gradient in the errors between higher and lower latitudes. However, it is evident from this figure that even in the ionosphere, errors in the higher-latitude portion of the magnetotail are much larger than those in the lower latitude region.

Because of the large size of the flux tubes that define each bin used in this error estimation and due to the limited number of data points within each flux tube, the method involves certain inaccuracies. However, all the features discussed above were observed in six independent data sets for the different versions of the T89 models. Thus we have strong confidence that the model properties found in this paper are real features, rather than artifacts produced by the chosen methodology. Furthermore, even though the results for only two different footpoint grid resolutions were discussed here, various others binnings were also examined. These revealed similar properties, so that the above results do not depend on the details of the chosen binning.

This work is an attempt to rigorously define errors contained in magnetic field models and field-aligned mappings. The method is relatively simple; any magnetic field model can be evaluated through a similar procedure. The results also show that this method is efficient in finding trends in data that would otherwise be difficult to detect.

Acknowledgments. This work was initiated at a magnetic field modeling workshop held at the Finnish Meteorological Institute in November 1994.

The Editor thanks one referee and G. D. Reeves for their assistance in evaluating this paper.

References

Acuña, M. H., K. W. Ogilvie, D. N. Baker, S. A. Curtis, D. H. Fairfield, and W. H. Mish, The global geospace science program and its investigations, in *The Global Geospace Mission*, edited by C. T. Russell, p. 5, Kluwer Acad., Dordrecht, the Netherlands, 1995.

Erickson, G. M., A quasi-static magnetospheric convection model in two dimensions, *J. Geophys. Res., 97*, 6505, 1992.

Fairfield, D. H., An evaluation of the Tsyganenko magnetic field model, *J. Geophys. Res., 96*, 1481, 1991.

Fairfield, D. H., N. A. Tsyganenko, A. V. Usmanov, and M. V. Malkov, A large magnetosphere magnetic field database, *J. Geophys. Res., 99*, 11319, 1994.

Hilmer, R. V., and G.-H. Voigt, A magnetospheric magnetic field model with flexible internal current systems driven by independent physical parameters, *J. Geophys. Res., 100*, 5613, 1995.

Iijima, T., and T. A. Potemra, The amplitude distribution of field aligned currents at northern high latitudes observed by Triad, *J. Geophys. Res., 81*, 2165, 1976.

Lockwood, M., and H. J. Opgenoorth, Opportunities for magnetospheric research using EISCAT/ESR and CLUSTER, *J. Geomagn. Geoelectr., 47*, 699, 1995.

Mead, G. D., and D. H. Fairfield, A quantitative magnetospheric model derived from spacecraft magnetometer data, *J. Geophys. Res., 80*, 523, 1975.

Newell, P. T., and C.-I. Meng, The cusp and the cleft/boundary layer: Low-altitude identification and statistical local time variation, *J. Geophys. Res., 93*, 14549, 1988.

Olson, W. P., and K. A. Pfitzer, Magnetospheric magnetic field modeling, *Annual Scientific Report, contract F44620-75-C-0033, Air Force Off. of Sci. Res.*, 96 pp., McDonnell Douglas Astronaut. Co., Huntington Beach, Calif., 1977.

Peredo, M., D. P. Stern, and N. A. Tsyganenko, Are existing magnetospheric models excessively stretched?, *J. Geophys. Res., 98*, 15,343, 1993.

Pulkkinen, T. I., D. N. Baker, R. J. Pellinen, J. Büchner, H. E. J. Koskinen, R. E. Lopez, R. L. Dyson, and L. A. Frank, Particle scattering and current sheet stability in the geomagnetic tail during the substorm growth phase, *J. Geophys. Res., 97*, 19,283, 1992.

Pulkkinen, T. I., D. N. Baker, R. J. Walker, J. Raeder, and M. Ashour-Abdalla, Comparison of empirical magnetic field models and global MHD simulations: The near-tail currents, *Geophys. Res. Lett., 22*, 675, 1995.

Pulkkinen, T. I., D. N. Baker, C. J. Owen, and J. A. Slavin, A model for the distant tail field: ISEE 3 revisited, *J. Geomagn. Geoelectr., 48*, 455, 1996.

Reeves, G. D., L. A. Weiss, and M. F. Thomsen, A quantitative test of different magnetic field models using conjunctions between DMSP and geosynchronous orbit, in Geophysical Monograph Series *Radiation belts*, edited by J.

Lemaire, D. Heynderickx, and D. N. Baker, AGU, Washington, D.C., in press, 1996.

Sergeev, V. A., M. Malkov, and K. Mursula, Testing the isotropic boundary algorithm method to evaluate the magnetic field configuration in the tail, *J. Geophys. Res., 98*, 7609, 1993.

Slavin, J. A., E. J. Smith, D. G. Sibeck, D. N. Baker, R. D. Zwickl, and S.-I. Akasofu, An ISEE-3 study of average and substorm conditions in the distant magnetotail, *J. Geophys. Res., 90*, 10,875, 1985.

Tsyganenko, N. A., Global quantitative models of the geomagnetic field in the cislunar magnetosphere for different disturbance levels, *Planet. Space Sci., 35*, 1347, 1987.

Tsyganenko, N. A., Magnetospheric magnetic field model with a warped tail current sheet, *Planet. Space Sci., 37*, 5, 1989.

Tsyganenko, N. A., Quantitative models of the magnetospheric magnetic field: Methods and results, *Space Sci. Rev., 54*, 75, 1990.

Tsyganenko, N. A., and A. V. Usmanov, Determination of the magnetospheric current system parameters and development of experimental geomagnetic field models based on data from IMP and HEOS satellites, *Planet. Space Sci., 30*, 985, 1982.

Tsyganenko, N. A., D. P. Stern, and Z. Kaymaz, Birkeland currents in the plasma sheet, *J. Geophys. Res., 98*, 19,455, 1993.

Yamamoto, T., K. Shiokawa, and S. Kokubun, Magnetic field structures of the magnetotail as observed by GEOTAIL, *Geophys. Res. Lett., 21*, 2875, 1994.

T. I. Pulkkinen, Finnish Meteorological Institute, P.O.Box 503, FIN-00101 Helsinki, Finland. (e-mail: tuija.pulkkinen@fmi.fi)

N. A. Tsyganenko, Hughes STX Corporation/NASA Goddard Space Flight Center, Code 695, Greenbelt, MD 20771. (e-mail: ys2nt@lepvax.gsfc.nasa.gov)

(Received March 5, 1996; revised May 14, 1996;
accepted August 6, 1996.)